Cirrus/Aerosols: Remote Sensing and Climatic Implication

K. N. Liou
Department of Atmospheric & Oceanic Sciences and
Institute of Radiation and Remote Sensing
University of California, Los Angeles

Outline

- A Global and microscopic View
- Remote Sensing of Thin Cirrus (and Aerosols)
- Climate Radiative Forcings of Cirrus (and Aerosols)

A Global View of Clouds from A GOES Satellite

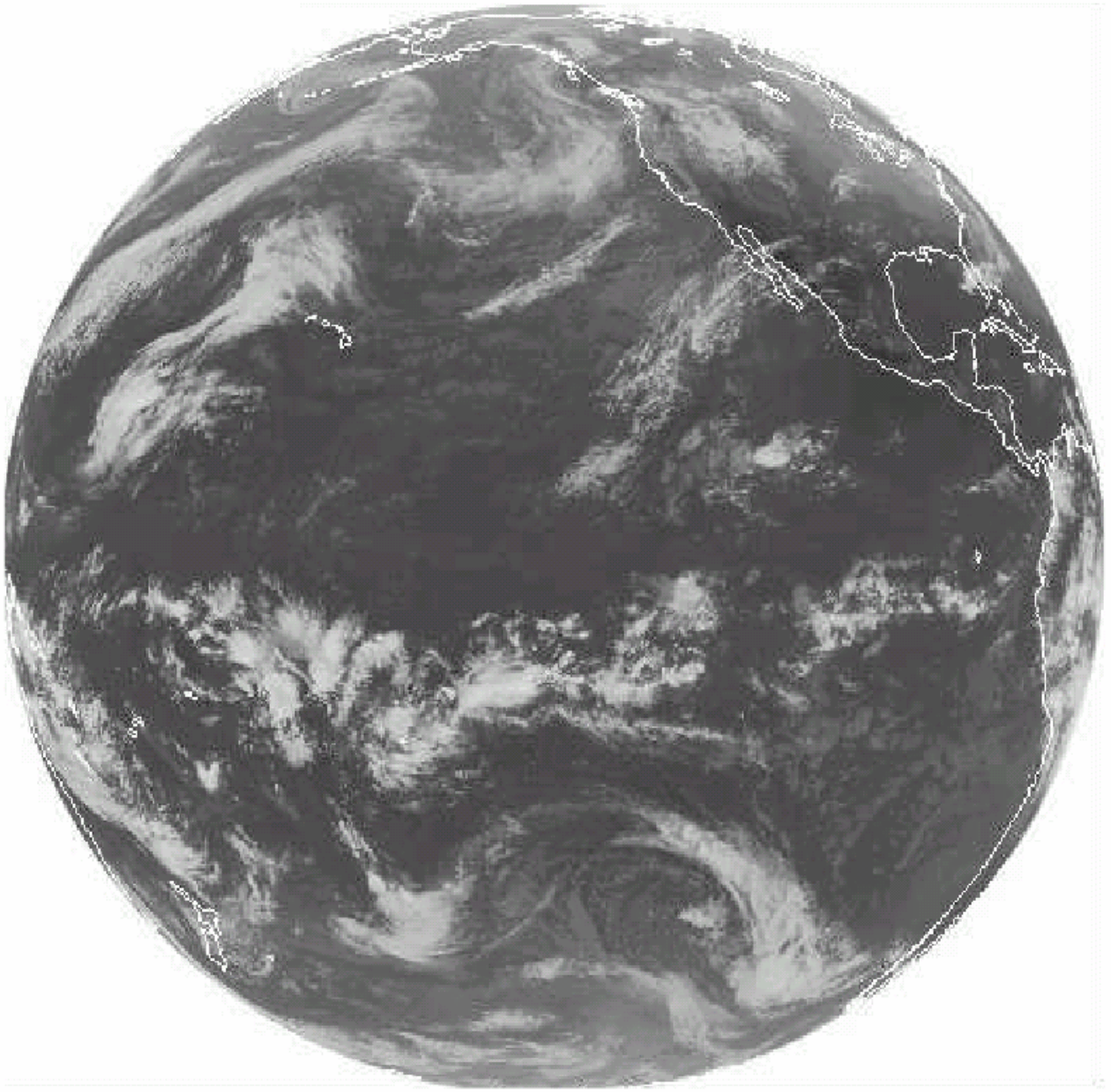

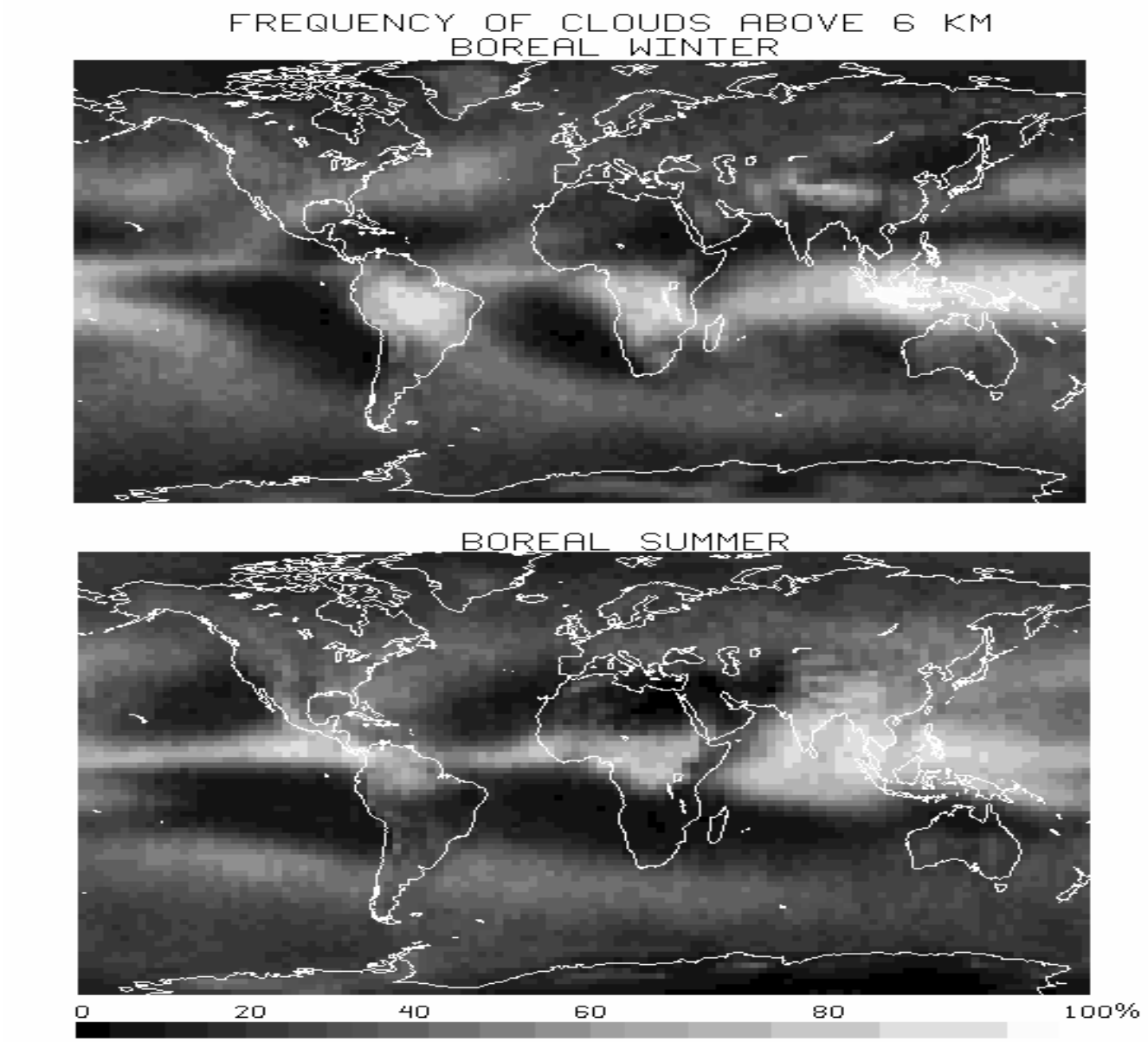

Figure 1. The frequency of clouds above 6 km detected from the HIRS data. Boreal winter is the months of December, January, and February, and boreal summer is the months of June, July and August (CO_2 slicing, 8 years). After Wylie and Menzel (1997)

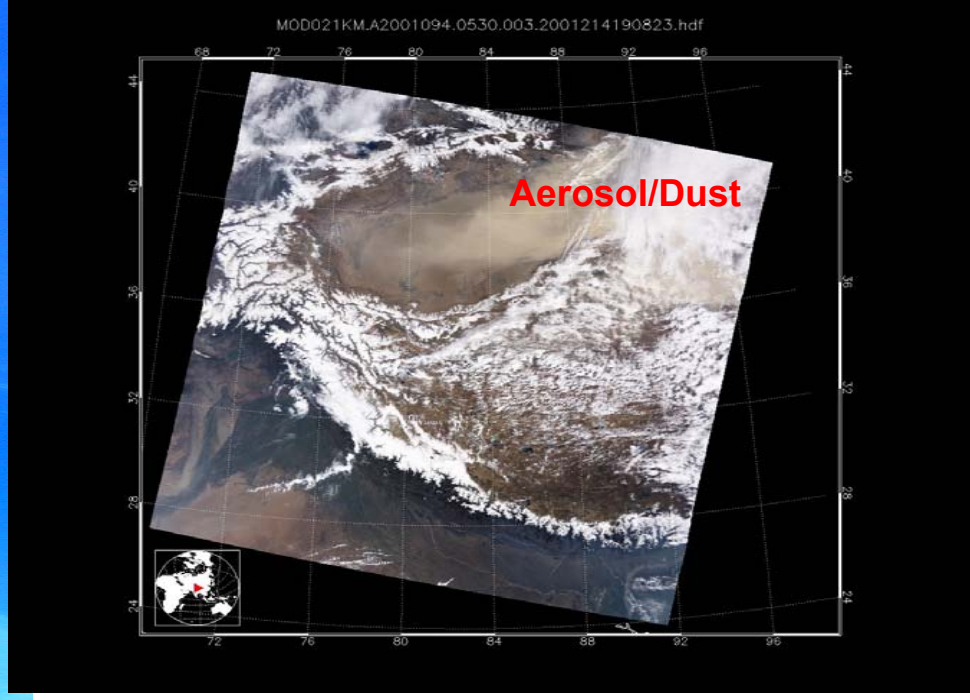

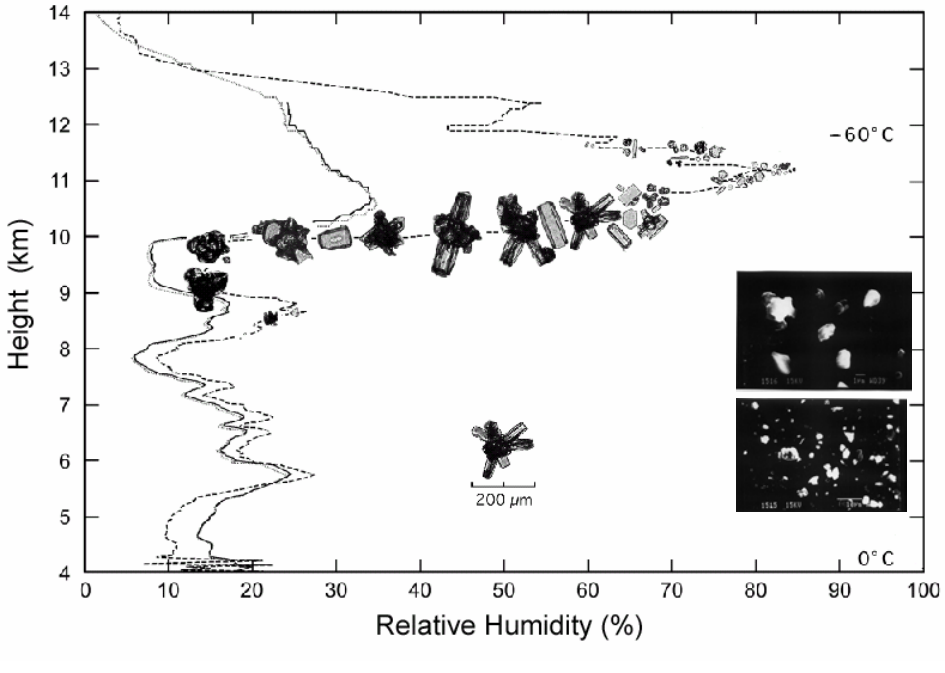

Radiative Transfer/A Unified Theory for Light Scattering by Ice Crystals and Aerosols

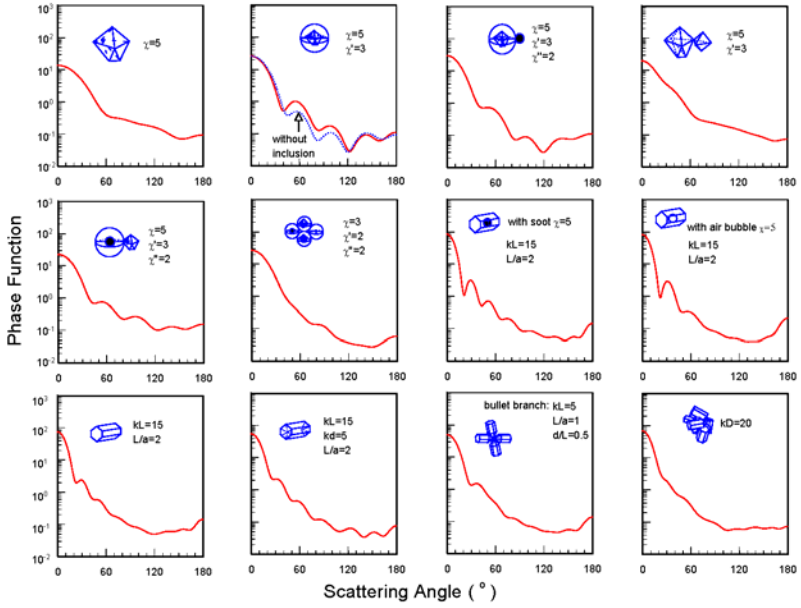

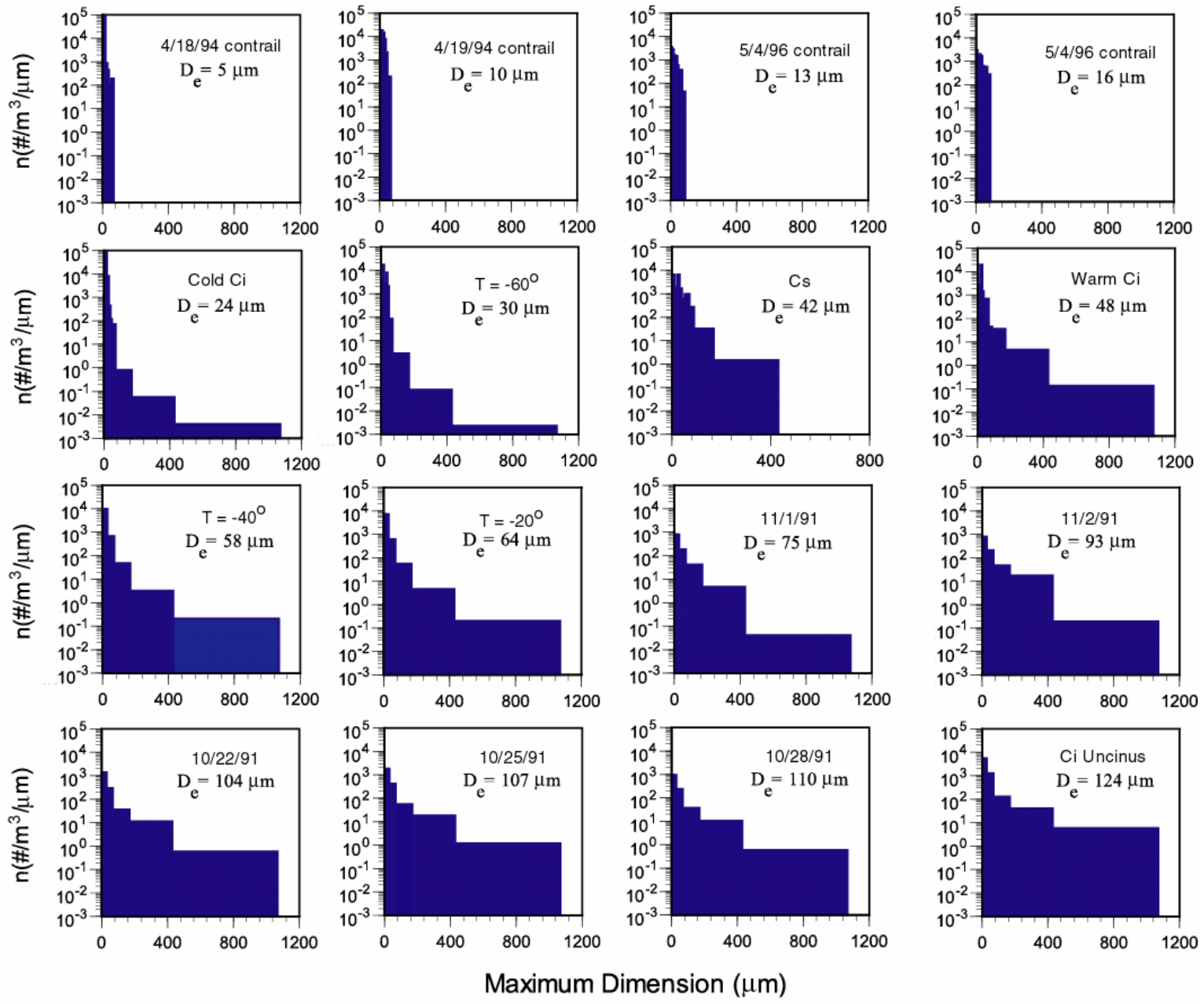

Fig. 1: Ice crystal size distributions for midlatitude cirrus cloud systems and contrails.

Remote Sensing of Thin Cirrus

- Detection and Separation of Thin Cirrus and Aerosols
- Thin Cirrus Information in the Emitted Line Spectra
- Ice Crystal Shape and Orientation Inferred from Polarization
- Three-Dimensional Cirrus Structure Inferred from Satellite and Mm-wave Radar

Simultaneous Retrieval of Thin Cirrus and Aerosol Optical Depth

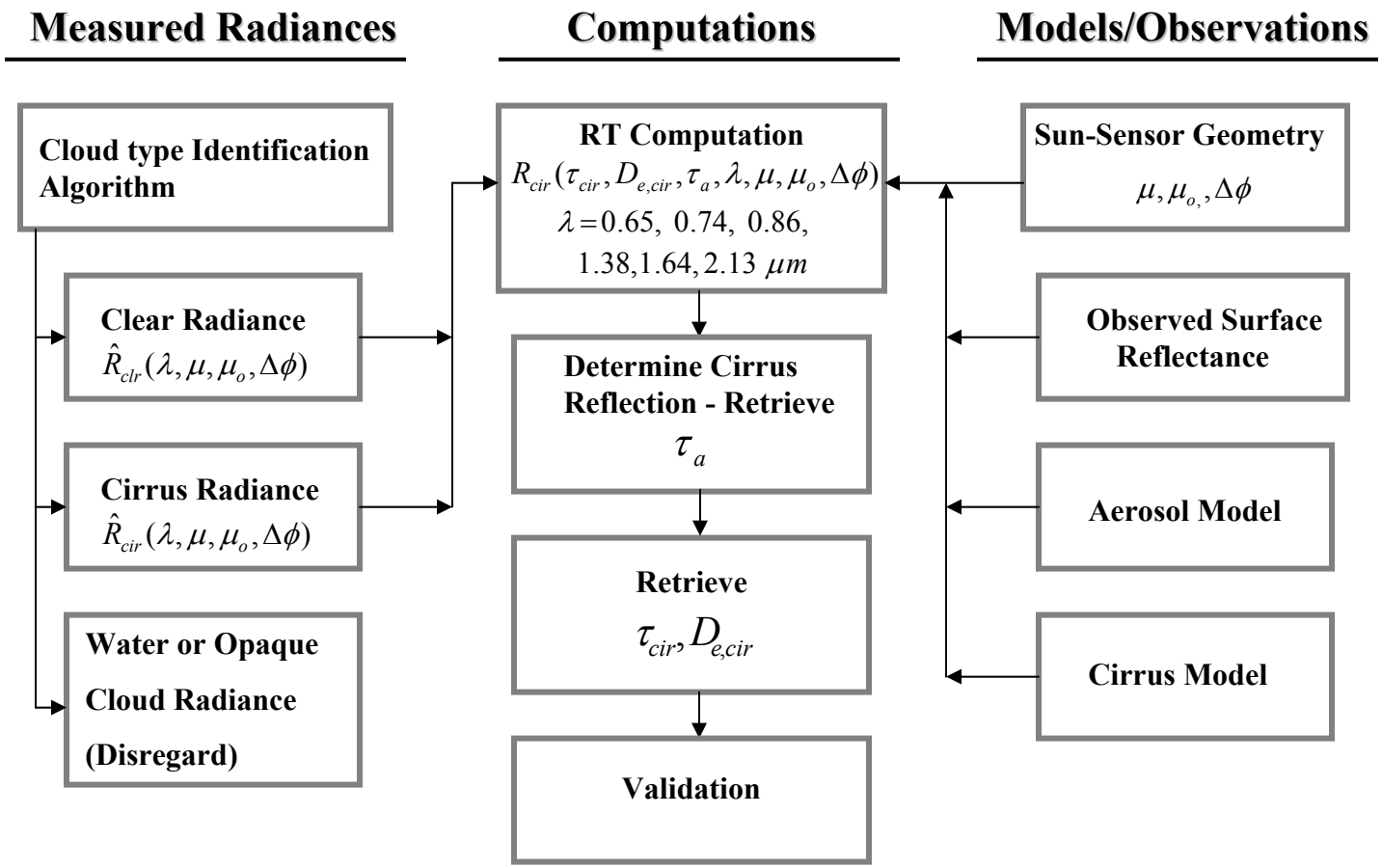

- Thin Cirrus Detection: Roskovensky and Liou (2003); 1.38/0.65 μm,& 8.6-11μm BTD
- Thin Cirrus and Aerosol Retrieval: Roskovensky, Liou, et al. (2004)

Comparison of Thin Cirrus Retrievals vs. In-Situ Measurements in Aerosol Atmospheres (Roskovensky and Liou, 2004)

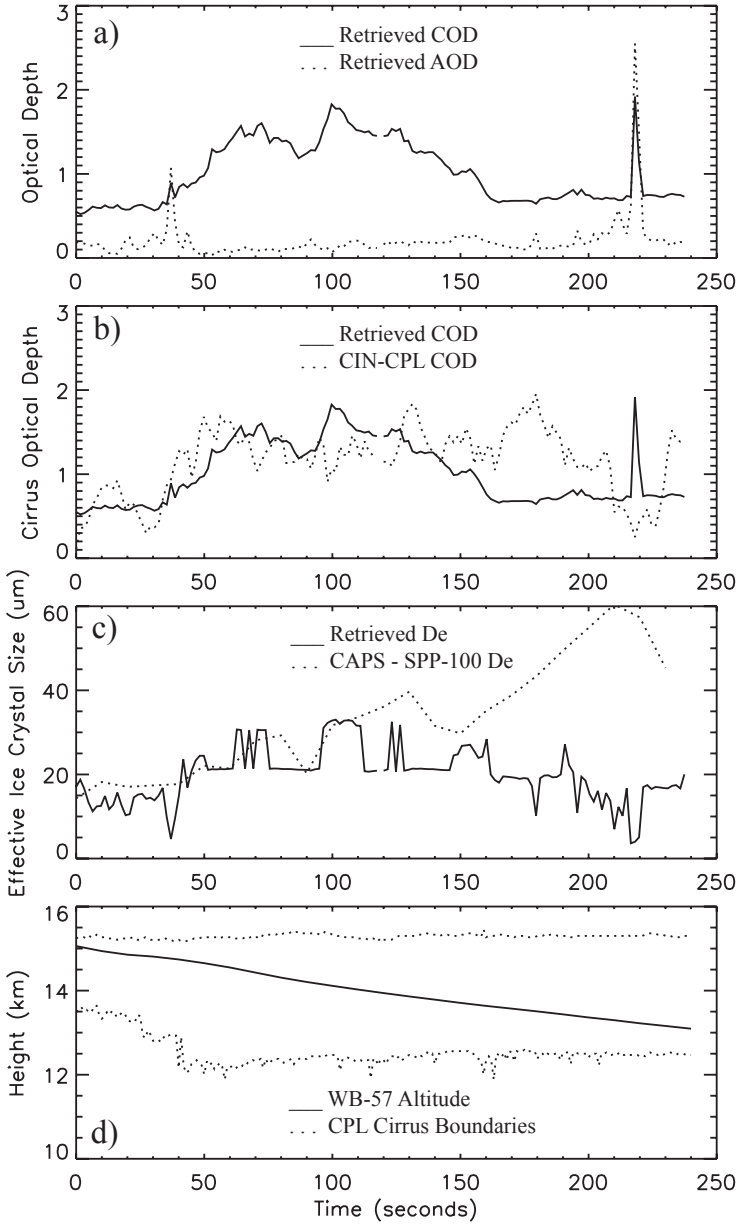

CRYSTAL-FACE July 26, 2002 (1859-1903 UTC)

ER-2 Aircraft Flight Path

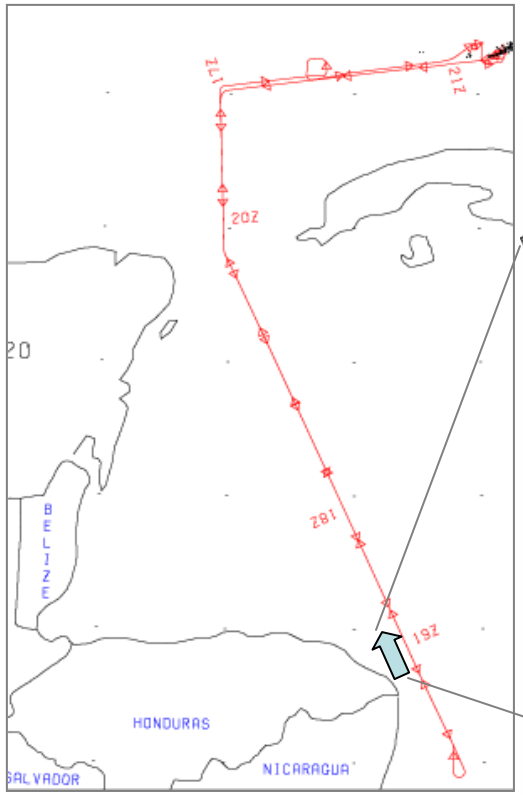

1.87 µm reflectance

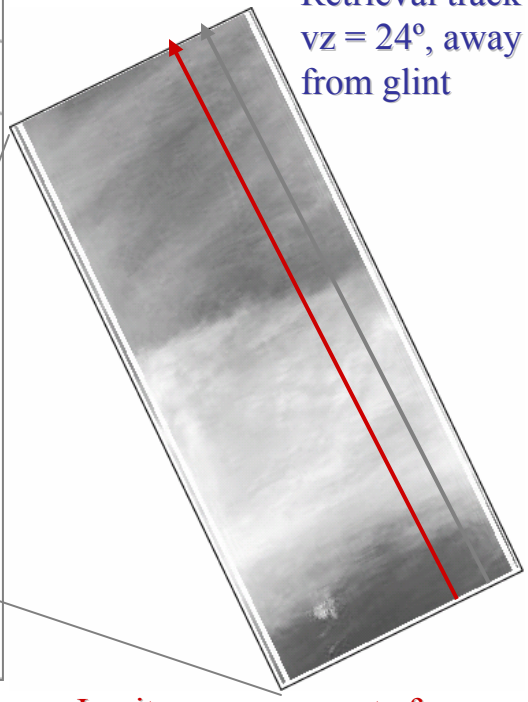

Retrieval track vz = 24°, away from glint

In-situ measurements from the WB-57. ~600m from retrieval track

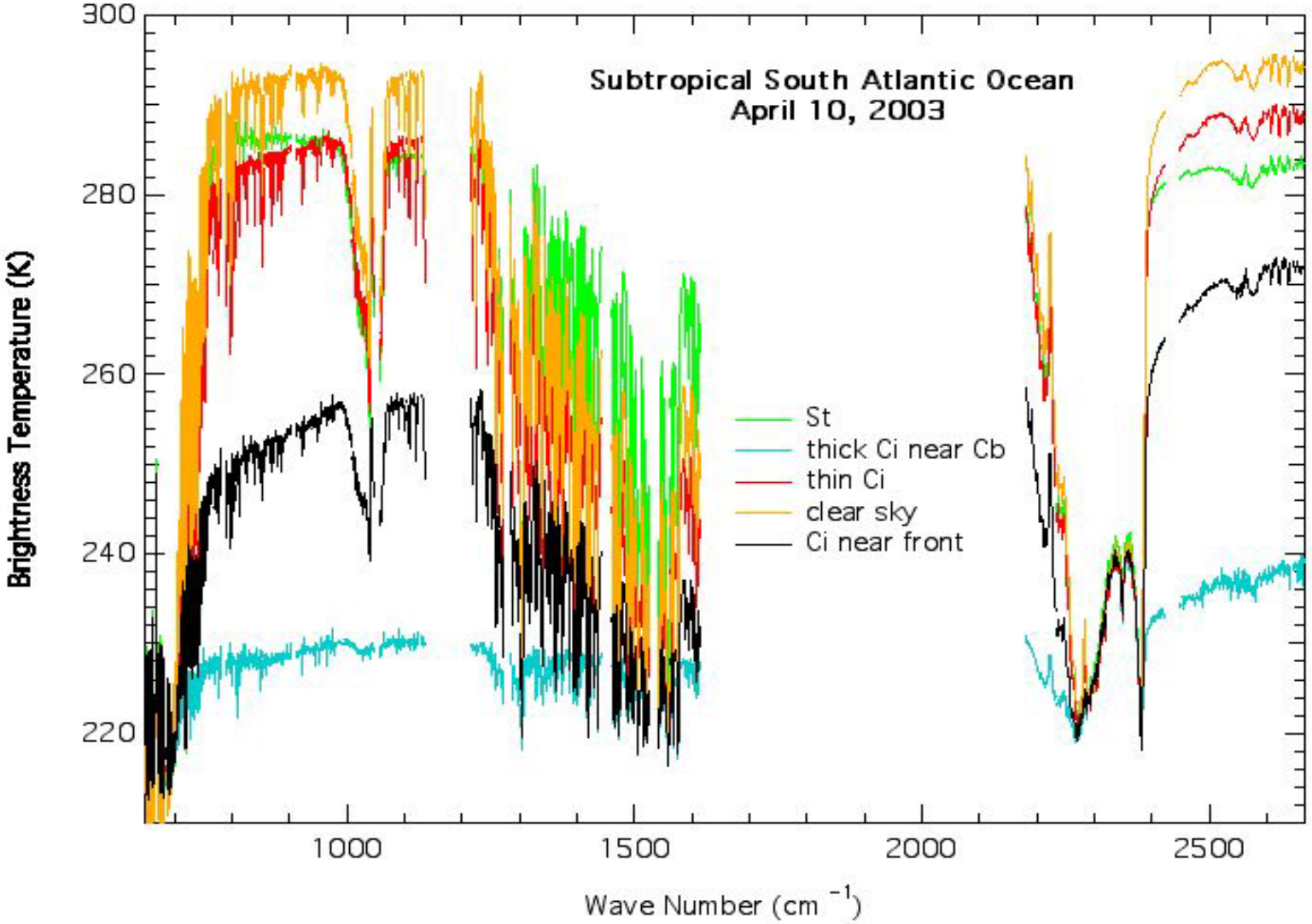

Figure 5. AIRS data measured on April 10, 2003, from 650 to 2700 cm^{-1} in a Subtropical South Atlantic cyclonic cloudy atmosphere in terms of brightness temperature. Kahn, Liou, et al. (2004) have developed a nighttime cirrus detection scheme based on the AIRS channels in the 10.4 and 3.8 μm (960-2616 cm^{-1}).

Interpretation of Cirrus Cloud Polarization Measurements: Ice Crystal Shape, Orientation, and (Size)

- Scattering Phase Matrix for Randomly (6 elements) and Horizontally (~8 elements) Oriented Plates, Solid and Hollow Columns, and Bullet Rosettes/Aggregates: A Unified Theory for Light Scattering by Ice Particles (Liou *et al.*, 2000)
- Stokes Vector Radiative Transfer in Anisotropic Ice Crystal Clouds: Adding/Doubling Method (Takano and Liou, 1989; Liou and Takano, 2002)
- Polarization Observations: Airborne Infrared Polarimeter (Coffeen, 1979; Chepfer *et al.*, 1999a, POLDER); POLDER on the ADEOS-1 Satellite Platform (Chepfer *et al.*, 1999b)

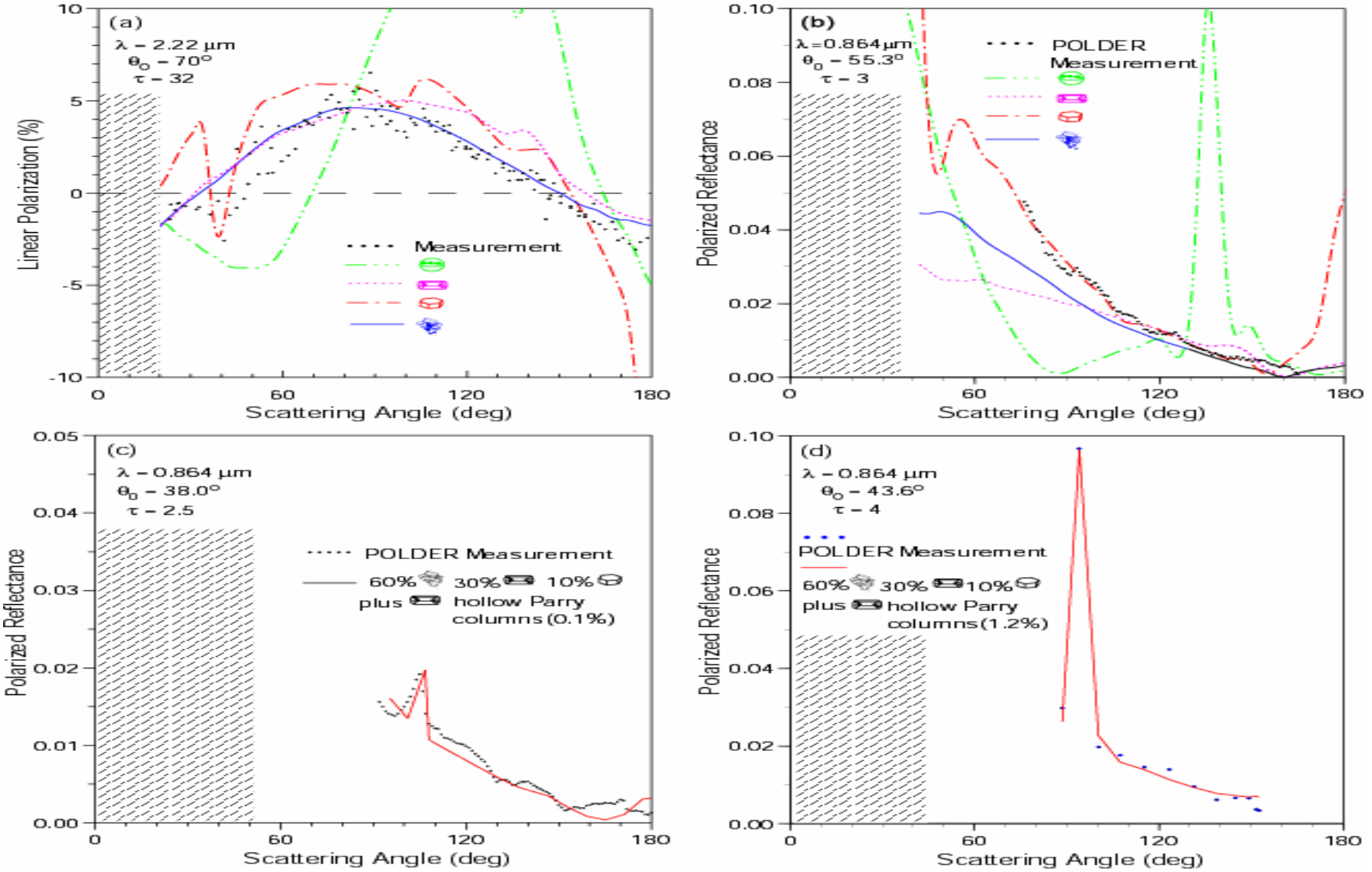

Figure 1. (a) Linear polarization of sunlight reflected from a cirrus measured by an airborne infrared polarimeter at 2.2 μm [Coffeen, 1979]. (b) and (c) Full polarization observed from an airborne POLDER instrument at 0.864 μm over an extended cirrus cloud system [Chepfer et al., 1999a]. (d) Same as (b) and (c) but on the ADEOS-1 satellite platform [Chepfer et al., 1999b]. The theoretical results are computed for randomly oriented hollow columns, plates, and irregular aggregates, and ice spheres. In (c) and (d), a small percentage of hollow Parry columns is added to produce the observed peaks. The shaded areas denote scattering angle regions where the reflected sunlight is out of the observation range for the solar zenith angles given in the figures (Liou and Takano, 2002; *Geophy. Res. Lett.*, **29**, 27-1 - 27-4).

Remote Sensing of 3-D Inhomogeneous Clouds

Combined Satellite and Mm-Wave Radar

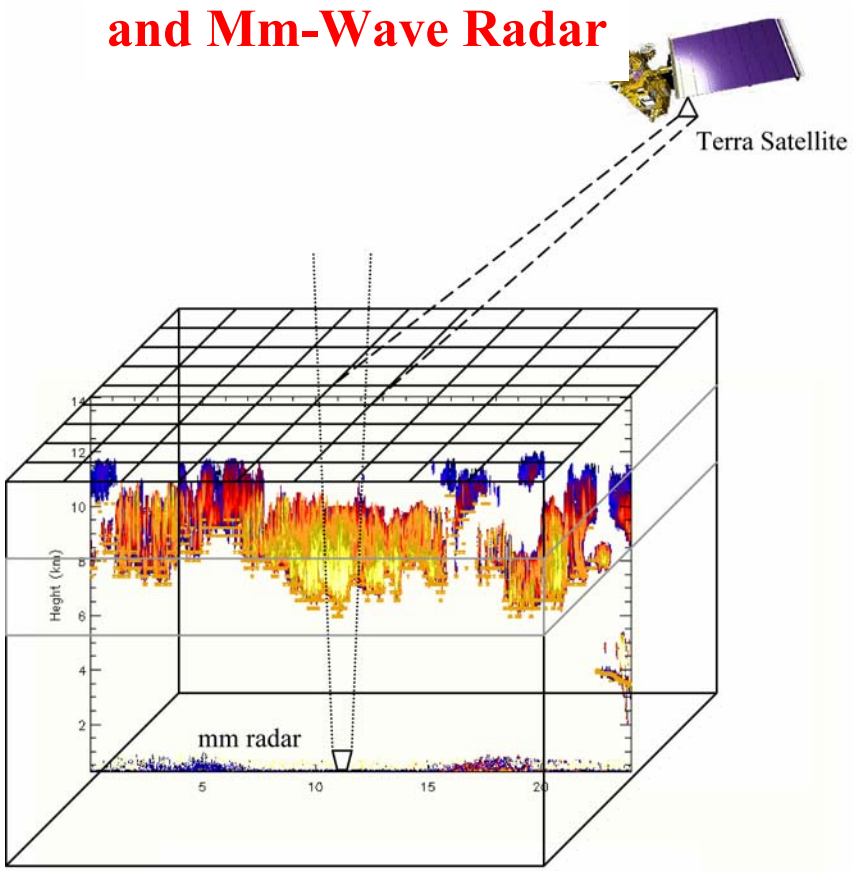

3-D Cloud Imaging in a Mesoscale Grid

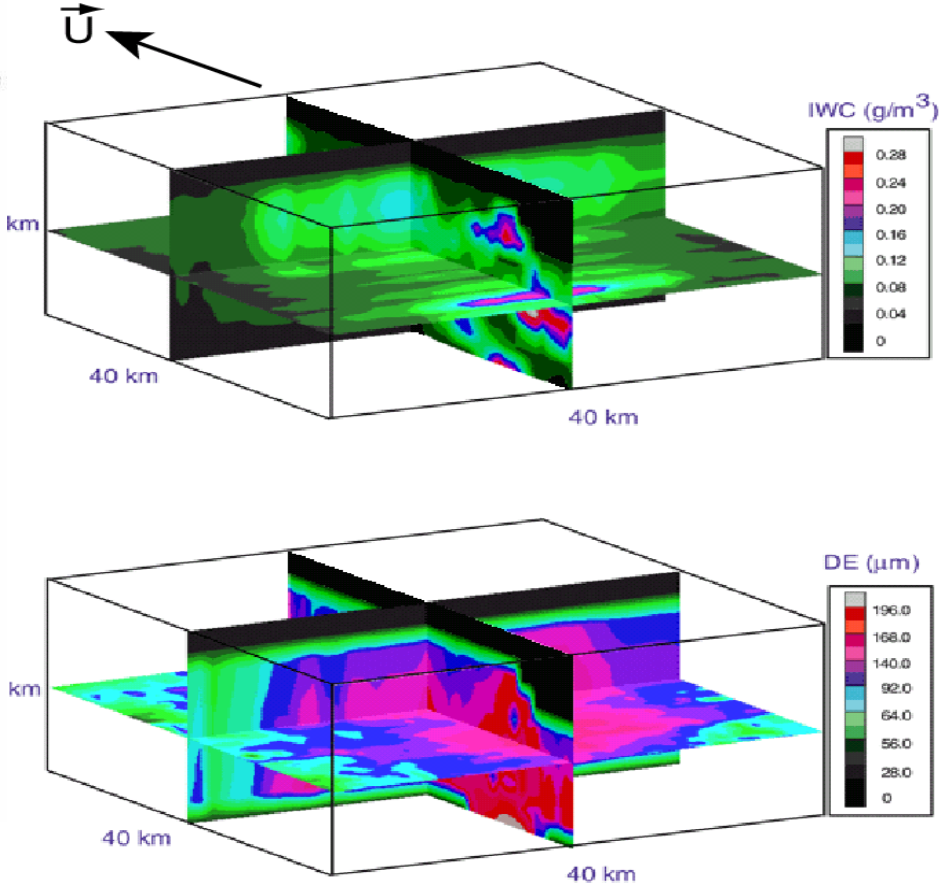

Construction of 3D Inhomogeneous Cloud and Radiation Fields

- Satellite : $\tau(\lambda,x,y)$, $\mathrm{DE}(x,y)$
- Ground-based Radar/Lidar data

  $\mathrm{IWC}(z,t) \rightarrow \mathrm{IWC}(x,z)$

  $\mathrm{DE}(z,t) \rightarrow \mathrm{DE}(x,z)$

  $x = ut$, u = wind speed, and t = measurement time
- Radiative Transfer Theory and Parameterization

  $\tau(\lambda,x,y) = \mathrm{IWC}(x,y)\Delta z(x,y)[a_0(\lambda) + a_1(\lambda)/\mathrm{DE}(x,y)\ ]$
- Normalized IWC and DE profiles

  $\mathrm{IWC}^*(x,z) = \mathrm{IWC}(x,z)/\overline{\mathrm{IWC}(x)}$

  $\mathrm{DE}^*(x,z) = \mathrm{DE}(x,z)/\overline{\mathrm{DE}(x)}$
- 3D Cloud Field

  $\mathrm{IWC}(x,y,z) = \mathrm{IWC}(x,y)\bullet\mathrm{IWC}^*(x,z)$

  $\mathrm{DE}(x,y,z) = \mathrm{DE}(x,y)\bullet\mathrm{DE}^*(x,z)$
- 3D Radiation Field

  $$\beta(\lambda,x,y,z) = \mathrm{IWC}(x,y,z)\sum_{n=0}^{N} a_n(\lambda)/\mathrm{DE}^n(x,y,z)$$

  $$1-\varpi(\lambda,x,y,z) = \sum_{n=0}^{N} b_n(\lambda)/\mathrm{DE}^n(x,y,z)$$

  $$g(\lambda,x,y,z) = \sum_{n=0}^{N} c_n(\lambda)\,\mathrm{DE}^n(x,y,z)$$

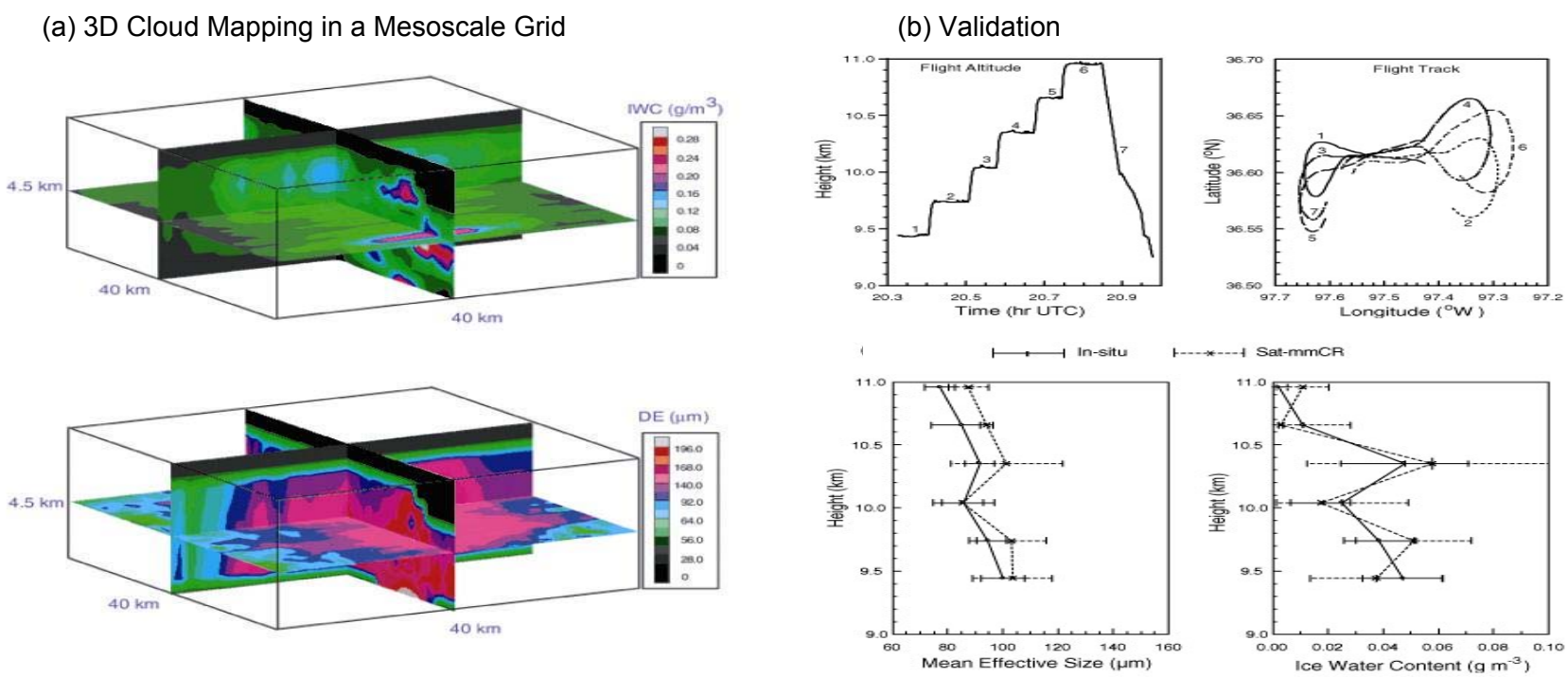

Figure 2 (a) Three-dimensional ice water content (IWC, 0-0.28 g/m^3) and mean effective ice crystal size (DE, 0-196 μm) determined from a unification of the optical depth and DE retrieval from the 0.63 and 3.7 μm AVHRR channels aboard the NOAA-14 satellite and the IWC and DE retrieved from the 35 GHz cloud radar over the ARM-SGP CART site at 2023 UTC on April 18, 1997. The 3D IWC and DE results are presented in *xy*, *yz*, and *xz* planes over a 40 km x 40 km x 4.5 km domain. **(b)** Time series of the flight altitude and the position of the flight track of the North Dakota Citation over the ARM-SGP CART site on April 18, 1997 (upper panel). Comparison of the mean (symbols) and standard deviations (bars) of the retrieved IWC and DE values from the unification approach involving satellite and cloud radar observations derived from *in situ* measurements taken on board the University of North Dakota Citation, as functions of aircraft leg height (lower panels) (Liou *et al.*, 2002).

Cloud Parameterization in Climate Models (Climate Simulations & Predictions)

- Cloud Cover/Position: Diagnostic/H_2O-field; Overlap
- Cloud Liquid/Ice Water Content (g/m^3): Prognostic Equations
- Cloud Particle Size (D_e/r_e): (Assumed)
- Cloud Inhomogeneity: (Subgrid Turbulence Theory; Data Analysis and Parameterization)

Remote Sensing of Clouds

- Cloud Cover/Type: ISCCP (VIS-IR 2-Channels)
- Cloud Liquid/Ice Water Path (g/m^2) } AVHRR/NOAA;
- Cloud Particle Size ($\overline{D}_e/\overline{r}_e$) } MODIS/Terra/Aqua
- Cloud Vertical Inhomogeneity
  Thin Cirrus: Detection and Retrieval

Cirrus and Climate

- **Cirrus and Greenhouse Warming: Temperature Dependence of IWC**
- **Contrail Cirrus: Direct and Indirect Effects**
- **Cirrus and Aerosol Indirect Effect**
- **Cirrus Radiative Forcing and a GCM Experiment**

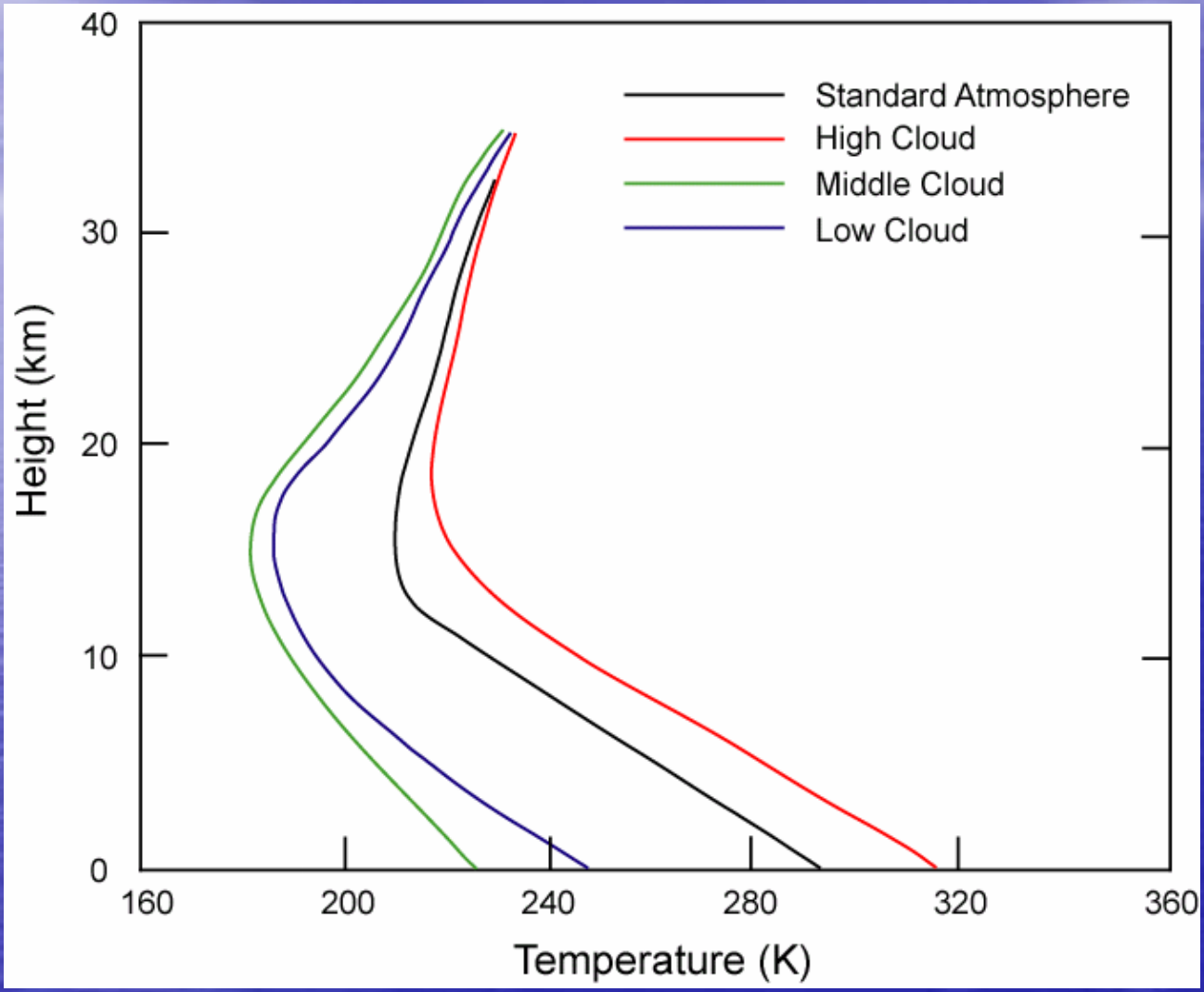

Fig. 8.14 Effects of high, middle, and low clouds on atmospheric temperatures in a radiative-convective model. The solid curve is the temperature profile of the standard atmosphere (data taken from Liou and Ou, 1983).

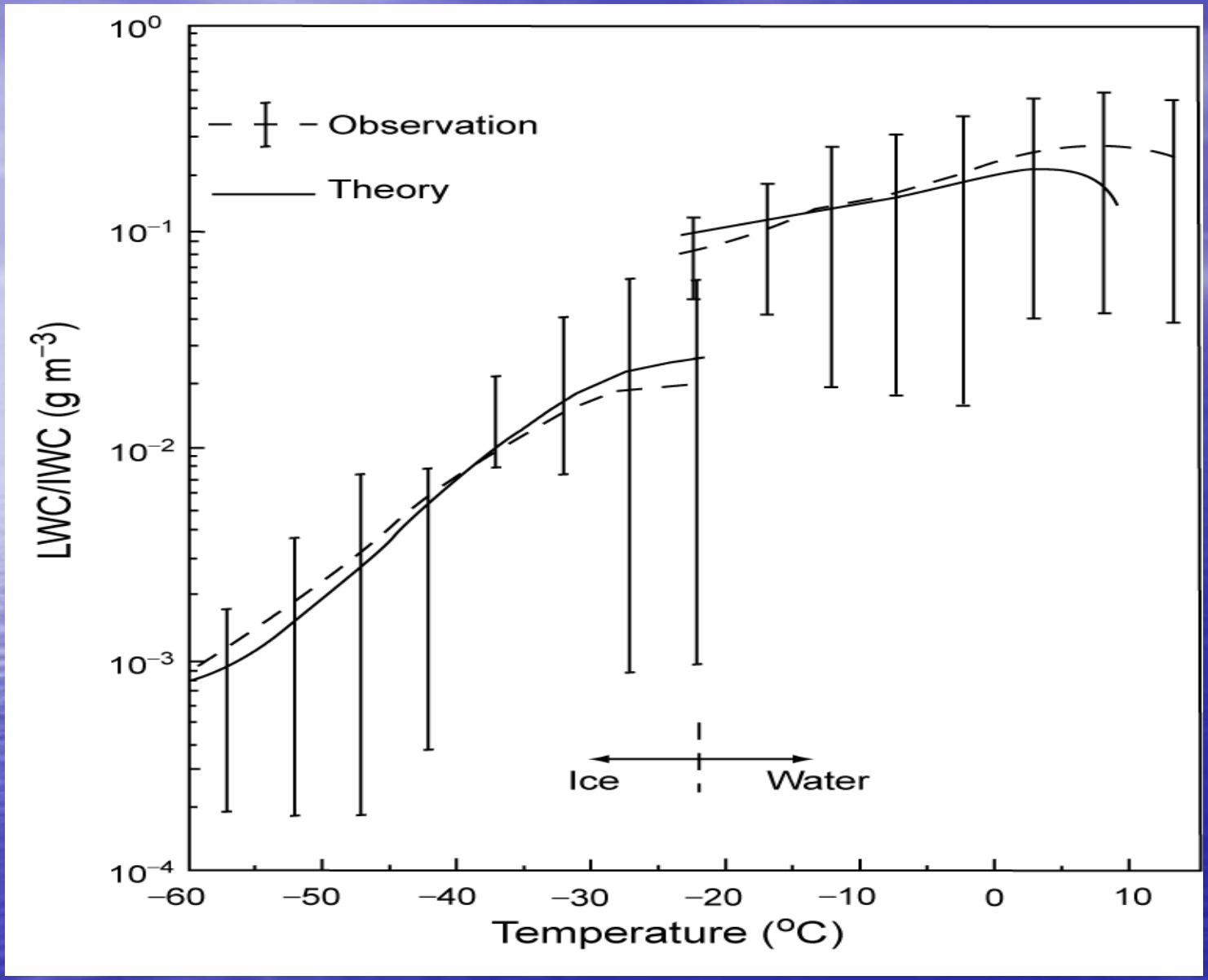

Fig. 8.15 Observed and model computed liquid water content (LWC) and ice water content (IWC) as functions of temperature. The observed LWC and IWC data are based on statistical averages of aircraft measurements presented by Matveev (1984) and Heymsfield and Platt (1984), respectively. Theoretical results are derived from diffusion and accretion models (after Liou 2002).

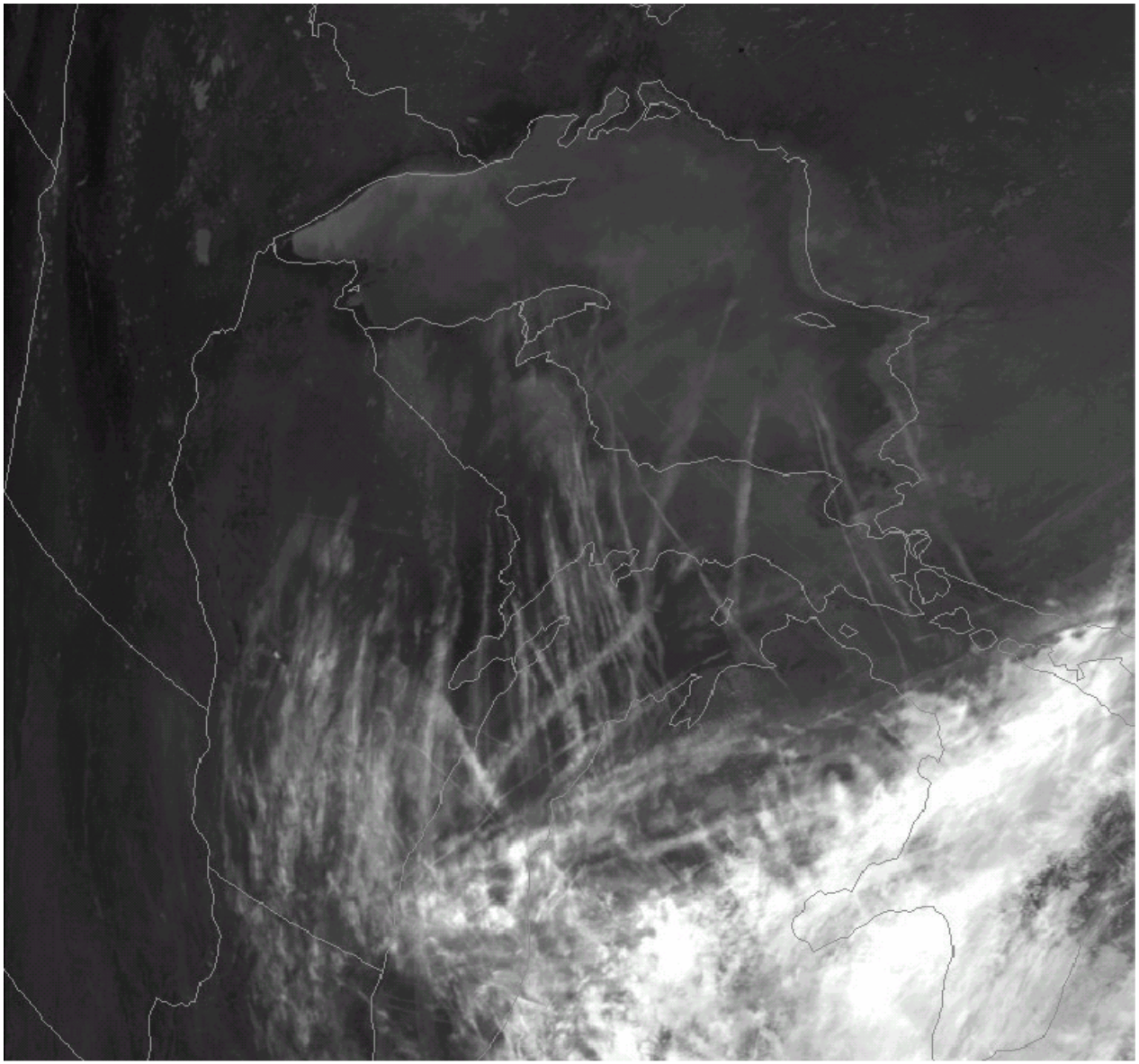

Fig. 8.28 High resolution thermal infrared image over the Great Lakes area of the United States from the NOAA-14 satellite at 2050 UTC October 2000, showing a number of north-south oriented contrails associated with patchy cirrus (courtesy of Patrick Minnis of the NASA Langley Research Center).

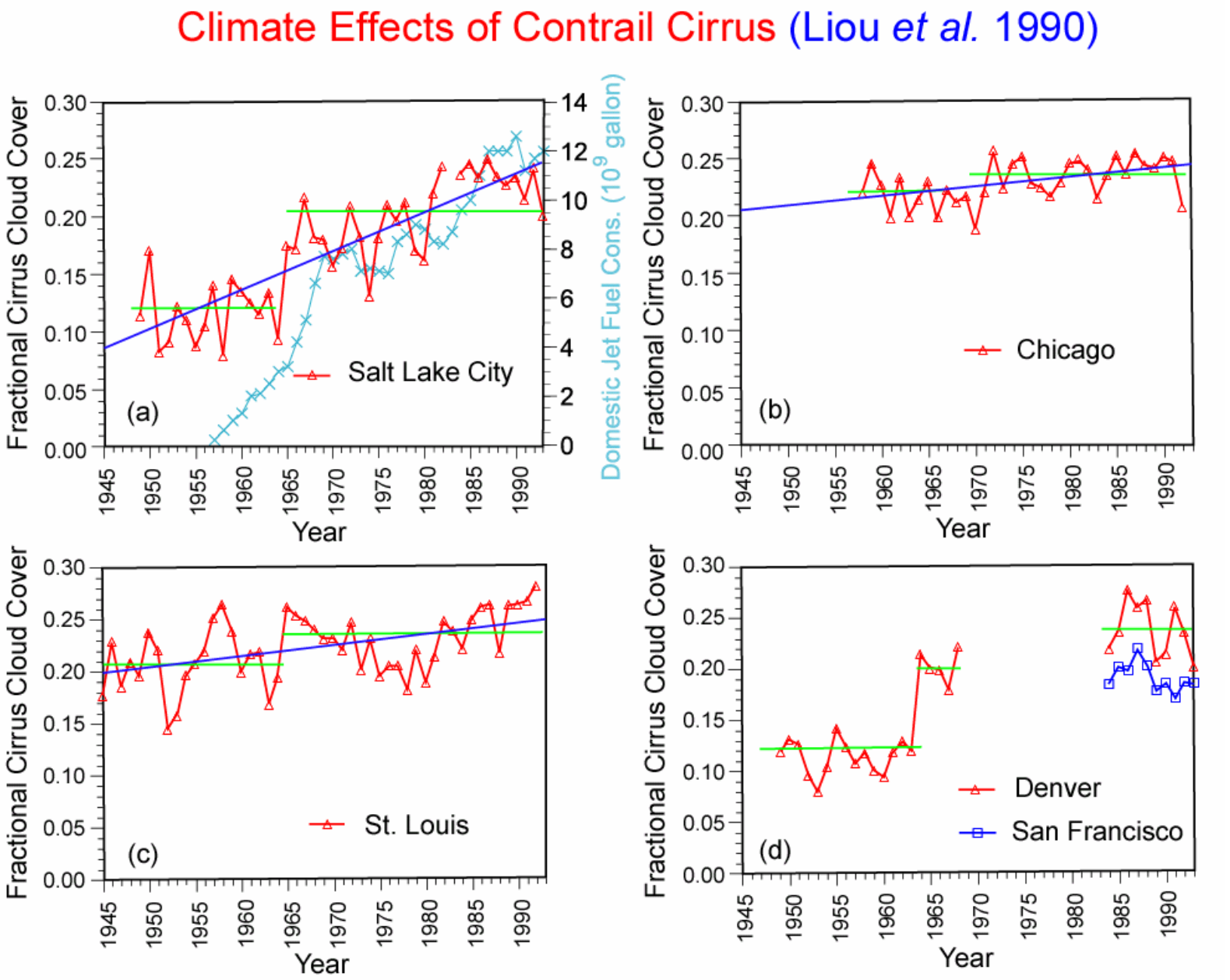

Figure 1. Cirrus cloud covers for a number of midlatitude cities from 1945 to 1992. Horizontal lines represent averages over respective periods. Also shown is the domestic jet fuel consumption.

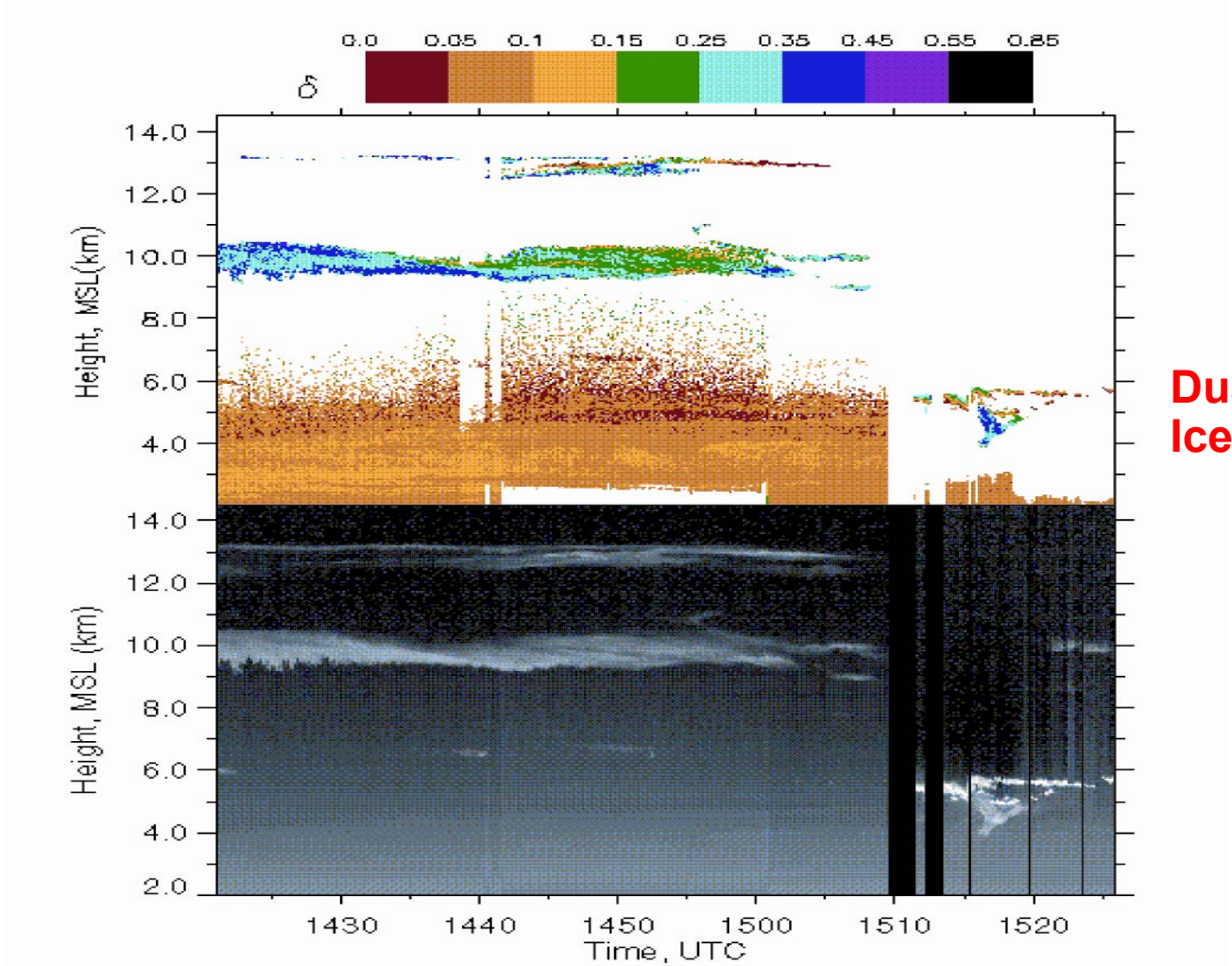

Dust-
Ice Clouds

Figure 1. PDL linear depolarization ratio (see color δ scale at top) and relative retrured power (in a logarithmic gray scale) height-versus-time displays on the morning of 29 July 2002, from the Ochopee field site of the CRYSTAL-FACE program. Note that low-altitude signals often cannot be used to calculate δ -values because of strong off-scale signals. Depicted are strongly depolarizing (δ ~ 0.2 to 0.4) upper troposheric cirrus clouds, aerosols (δ ~ 0.10 to 0.15) extending up to ~5.5 km, and at far right a super cooled liquid altocumulus cloud ($\delta \approx 0$ at cloud base). Note the temporary glaciation of this cloud as it descended into the top of the dust layer (after Sassen et al. 2002).

Spectral Line-By-Line-Equivalent Radiative Transfer Program

- Adding/Doubling Method for Radiative Transfer (Takano and Liou, 1989)
- Correlated k-distribution Method for Gaseous Absorption in Multiple Scattering Inhomogeneous Atmospheres (Fu and Liou, 1993; Liou et al., 1998)
- Molecular Absorption and Sources (Rothman et al., 2000 and others)
- Solar Spectrum (MODTRAN 3.7) and Solar Constant (1366 W/m^2, Lean and Rind, 1998)
- Light Scattering by Aerosols (d'Almeida et al., 1991), Water Droplets, and Ice Crystals (3D & 2D Orientation; Liou, Takano, and Yang, 2000); Rayleigh Scattering; and Surface Reflection

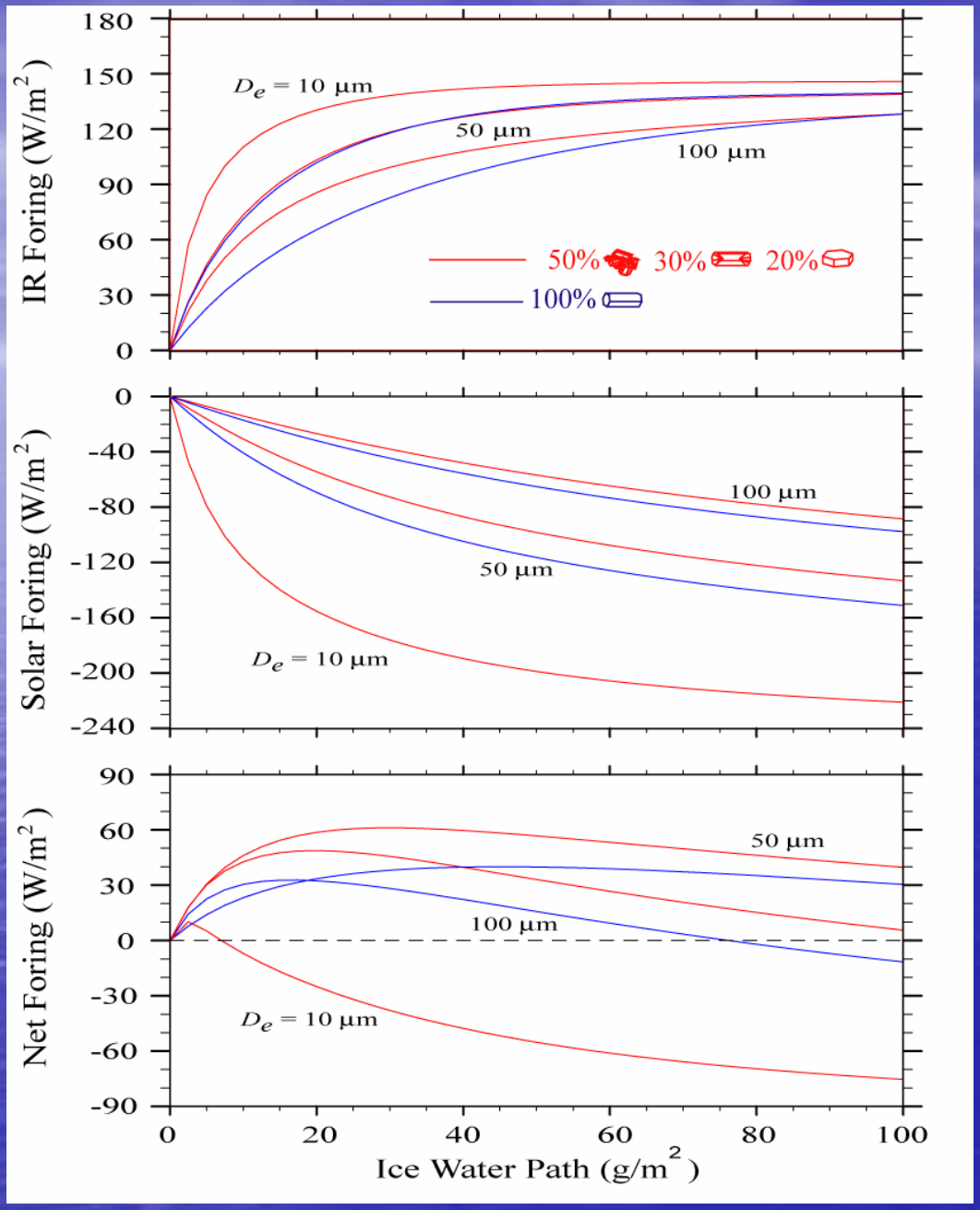

Cloud Radiative Forcing

$$C_{s,ir} = F_{s,ir}^{clear} - F_{s,ir}^{cloud}$$

Figure 1. Solar, IR, and net radiative forcings for cirrus clouds as functions of mean effective size D_e and ice water path for two ice crystal shape distributions in the standard atmospheric condition. The solar constant, solar zenith angle, surface albedo, cloud base height, and cloud thickness used in the calculations are 1366 W/m^2, 60^o, 0.1, 9 km, and 2 km, respectively.

Table 1. Global Cloud Radiative Forcing (W/m^2) Observed from the ERBE Satellite[@] and Calculated from an Improved Fu-Liou Broadband Radiation Program*

	Solar	IR	Net
Observed from ERBE	**-48.40**	**31.05**	**-17.25**
Calculated from ISCCP*	**-47.76**	**30.43**	**-17.33**
Add 10% thin cirrus ($\tau_v = 0.03$)	**-47.83** (-0.07)	**30.65** (+0.22)	**-17.18** (+0.15)
Add 10% cirrus ($\tau_v = 0.1$)	**-48.01** (-0.25)	**31.14** (+0.71)	**-16.87** (+0.46)

[@]After Harrison et al. (1990)

*ISCCP: high clouds, 14.0%; middle clouds, 18.2%; low clouds, 25.4%; clouds are randomly overlapped; LWP = 40 g/m^2, r_e = 10 μm; IWC = 20 g/m^2, D_e = 75 μm; US standard atmosphere; $\mu_o = 0.5$; $A_s = 0.1$.

Remote Sensing and Radiative Forcing Analysis: Tropical Ocean (ARM TWP Site)

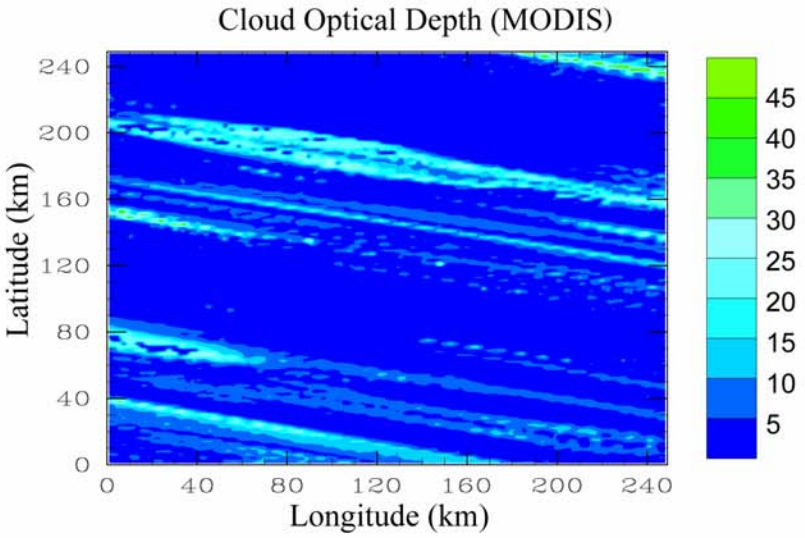

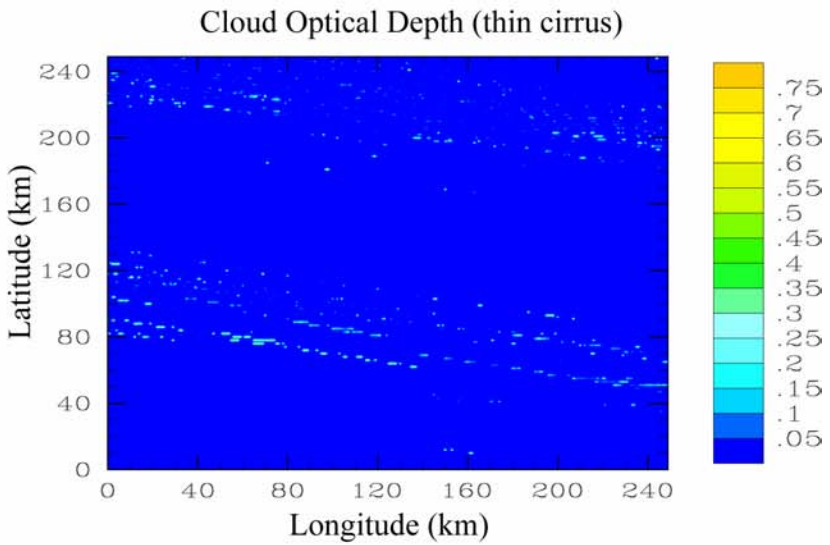

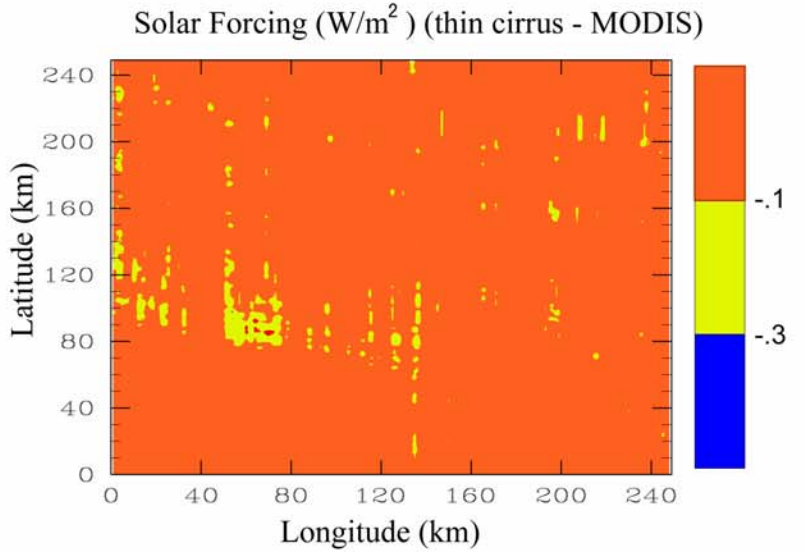

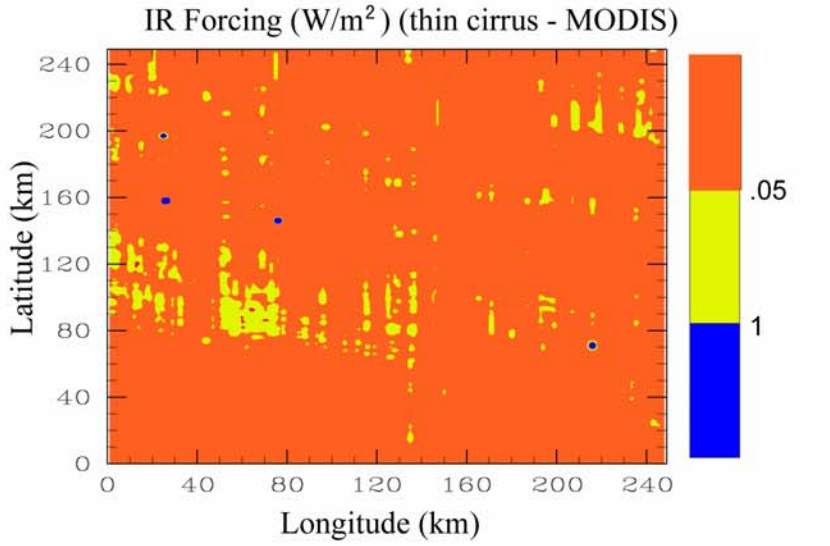

UCLA AGCM

- **Physical Parameterizations**

  Planetary boundary layer processes: Suarez et al. (1983), Li et al. (1999, 2001)

  Cumulus convection: Prognostic Arakawa-Schubert (Pan and Randall 1998) with downdrafts (Cheng and Arakawa 1997)

  Radiation: Fu and Liou (1992, 1993), Gu and Liou (2001, inhomogeneity; 2004, aerosols)

  Prognostic cloud water/ice: Kohler (1999) + Fractional clouds/cloud overlap (Gu, Liou, et al. 2003)

  Gravity water drag: Kim and Arakawa (1995)

- **Dynamics**

  Horizontal finite difference scheme: Arakawa and Lamb (1981)

  Resolution: 5° longitude x 4° latitude

  Vertical finite difference scheme: Suarez and Arakawa (1983)

  Resolution (top at 1 hPa): 15 layers

  Time integration: Leapfrog, Matsuno

- **Surface Conditions**

  Prescribed sea surface temperatures (Rayner et al. 1995), albedo, ground wetness, and surface roughness (Dorman and Sellars 1989)

Climate Impact of a 10 % Increase in High Cloud Cover

ΔOLR

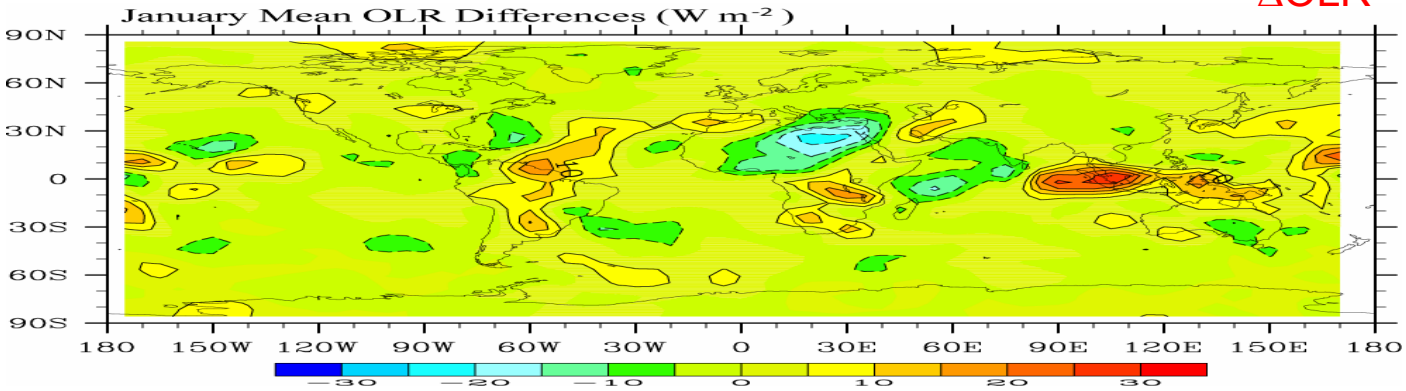

ΔT_s

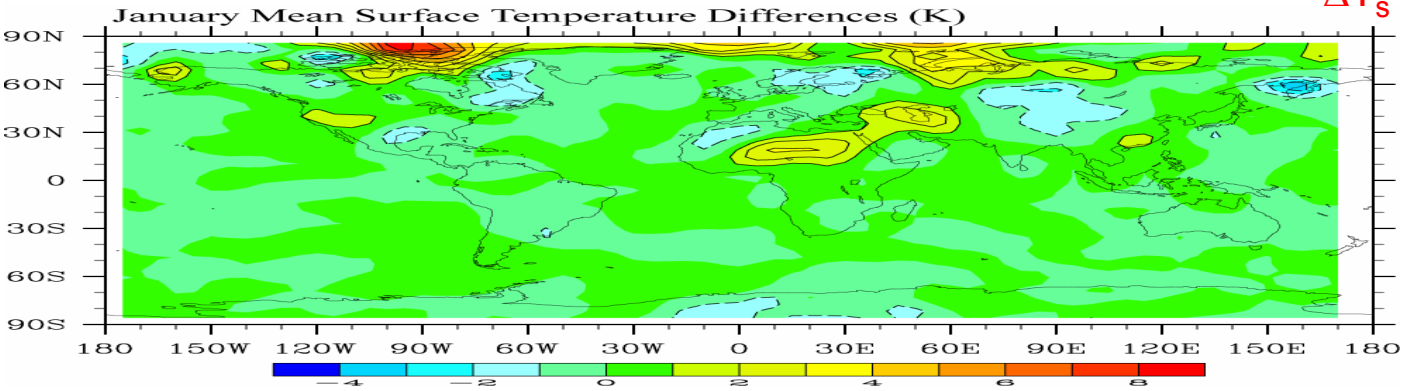

ΔP

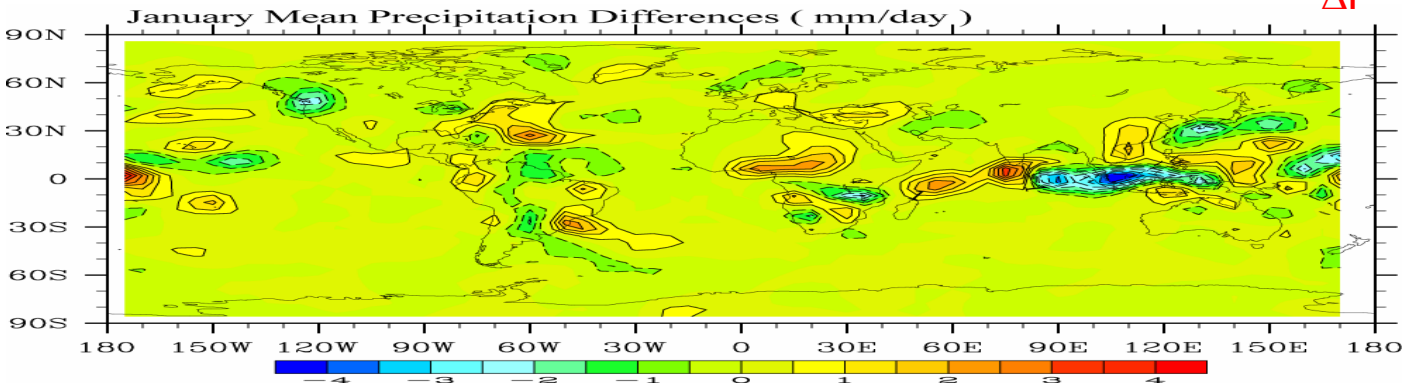

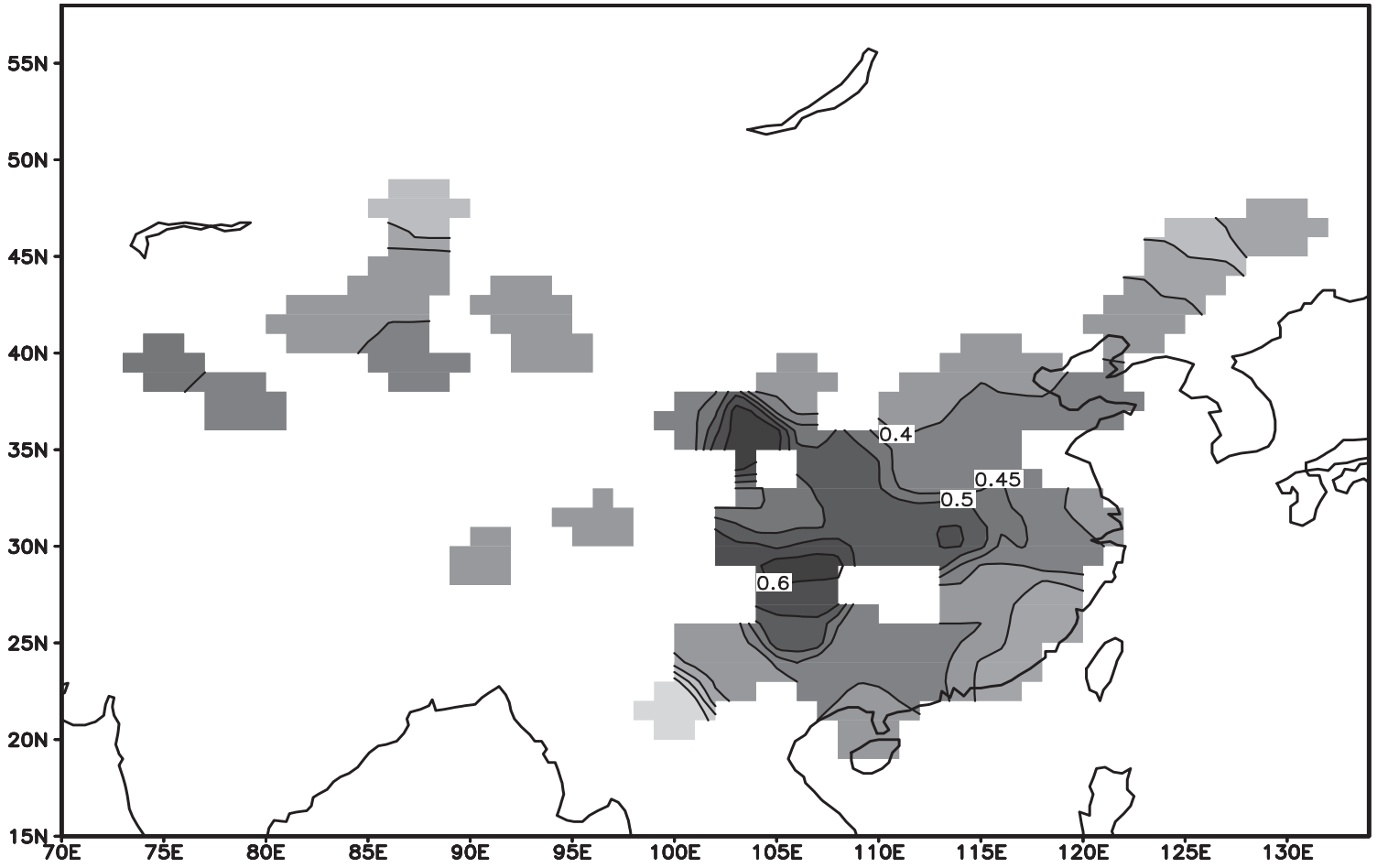

Fig. 1. The observed mean January optical depth in China.

Aerosol Optical-Depth Effect on Precipitation: A UCLA GCM Study (Gu, Liou, et al., in preparation)

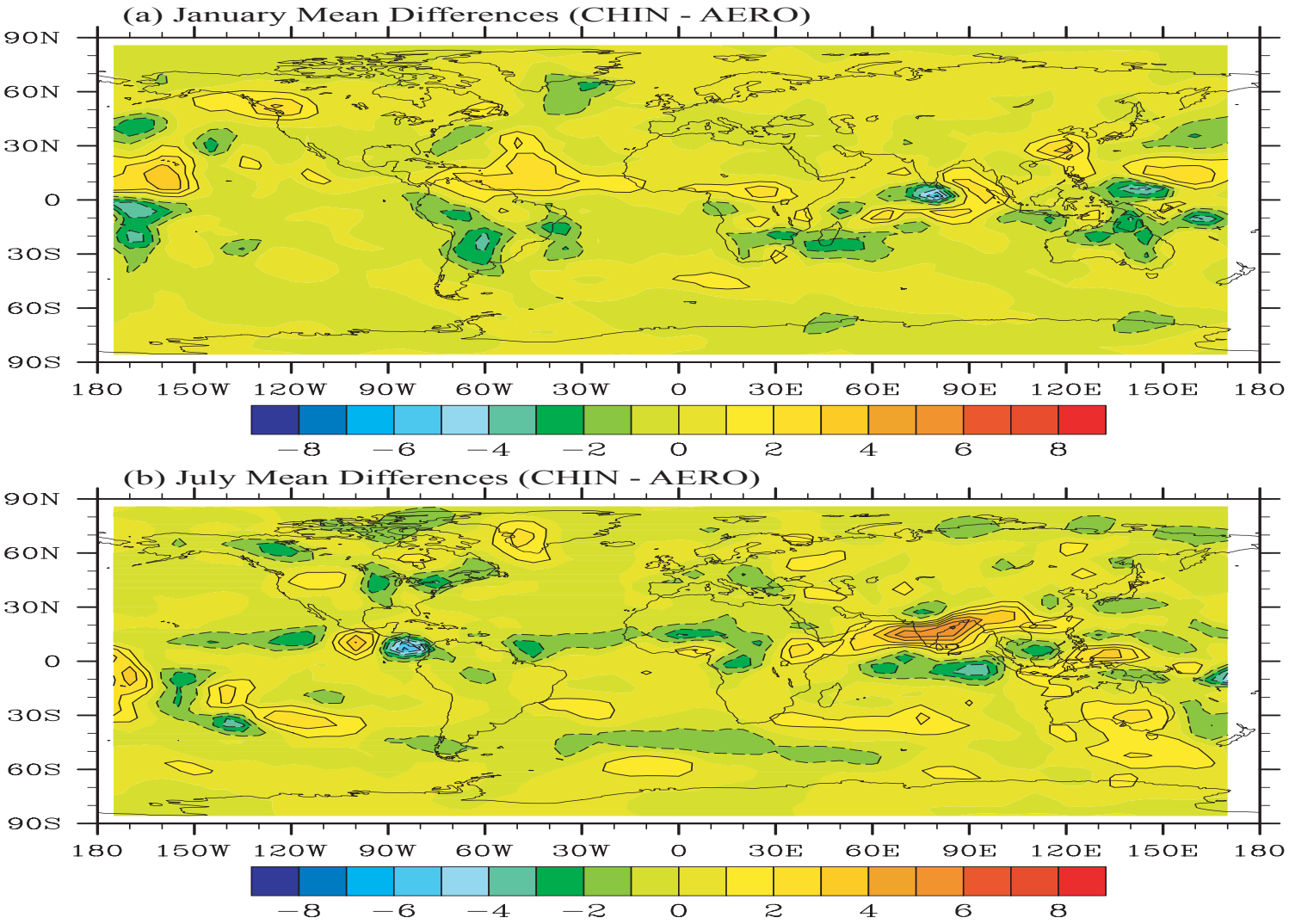

Cirrus/Aerosols: Remote Sensing and Climatic Implication

K. N. Liou
Department of Atmospheric & Oceanic Sciences and
Institute of Radiation and Remote Sensing
University of California, Los Angeles

Outline

- A Global and microscopic View
- Remote Sensing of Thin Cirrus (and Aerosols)
- Climate Radiative Forcings of Cirrus (and Aerosols)